# CHAPTER 5

# KINETIC MODEL OF NITROGEN ABSORPTION AND DESORPTION DURING WELDING

As discussed in §1.4.2, the results reported by Kuwana *et al*[1] suggest that a kinetic approach may be more appropriate than a thermodynamic method for describing the dissolution of nitrogen in high chromium alloy and stainless steel welds. In order to combine the results described in the previous chapter in a suitable theoretical framework, a kinetic model was developed to describe the absorption and evolution of nitrogen during the welding of stainless steel. The ultimate aim of the model is to predict the maximum amount of nitrogen that can be accommodated in the shielding gas before the onset of steady-state behaviour associated with degassing and nitrogen bubble formation. This will facilitate the addition of limited amounts of nitrogen to argon shielding gas during the autogenous welding of nitrogen-strengthened stainless steels, thereby preventing the nitrogen losses generally associated with autogenous welding of these alloys. Maintaining the shielding gas nitrogen content below the saturation level will prevent the formation of nitrogen-induced porosity during autogenous welding in practice.

## 5.1 OUTLINE OF THE KINETIC MODEL

The kinetic model is based on the following assumptions:

(a) Nitrogen enters the molten weld pool from two sources:

- the arc atmosphere, i.e. the dissolution of monatomic and diatomic nitrogen from the arc plasma into the liquid metal, and
- the nitrogen-containing base metal that melts at the leading edge of the weld pool during autogenous welding.

(b) Dissolved nitrogen is removed from the weld pool by:

- recombining to form nitrogen molecules which can escape to the atmosphere, and
- solidification of nitrogen-containing weld metal at the rear of the weld pool.

(c) Under steady-state conditions a state of dynamic equilibrium is created whereby the amount of nitrogen entering the weld pool is equal to the amount of nitrogen leaving the weld pool per unit time.

(d) The molten weld pool is completely covered by plasma using the welding parameters described in §3.2.

(e) The rate of solidification of the weld metal at the rear of the weld pool is proportional to the welding speed.

(f) Due to rapid convection in the molten weld metal, the pool is well mixed with a uniform nitrogen concentration. Rapid mass flow in the weld pool also ensures a fairly homogeneous temperature distribution in the molten metal during welding.

(g) The model is only valid under conditions where the evolution of nitrogen occurs at the weld pool surface and no bubble formation takes place in the weld metal.

The model is illustrated schematically in Figure 5.1 and considered below in more detail.

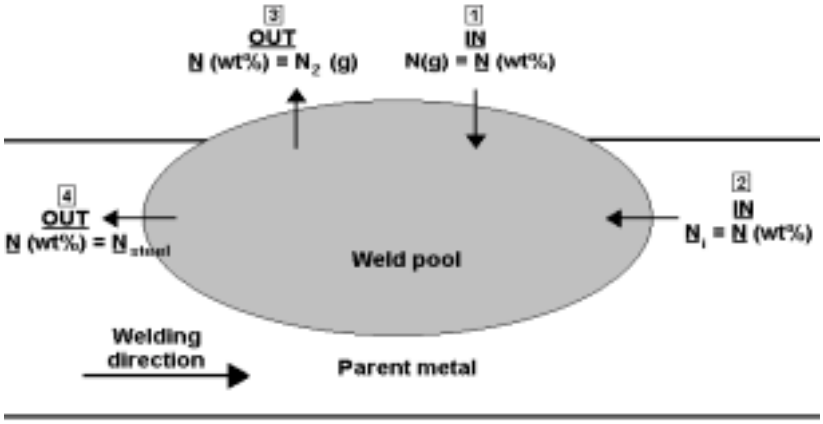


**Figure 5.1** Schematic illustration of the proposed kinetic model for the absorption and desorption of nitrogen from autogenous stainless steel weld metal.

The proposed rate equations for the four processes responsible for nitrogen entering and leaving the molten weld pool, as illustrated in Figure 5.1, are given below:

(1) Nitrogen entering the weld pool from the arc atmosphere:

The absorption of monatomic nitrogen from the arc plasma, reaction (5.1), is best described by a first order rate equation, with the rate of mass transfer for this reaction represented by equations (5.2) and (5.3). Rewriting this expression in terms of mass percentages yields equation (5.4).

$$\mathrm{N\,(g)} \rightarrow \underline{\mathrm{N}}\,(\mathrm{wt\%}) \qquad \ldots(5.1)$$

$$\frac{dm_N}{dt} = Ak[N(g) - N_{eq}(g)] \qquad \ldots(5.2)$$

$$\therefore \quad \frac{dm_N}{dt} = Ak\left[N(g) - \frac{N_{steel}}{K}\right] \qquad \ldots(5.3)$$

$$\therefore \quad \frac{d\underline{N}(wt\%)}{dt} = \frac{100Ak}{\rho V}\left[N(g) - \frac{N_{steel}}{K}\right] \qquad \ldots(5.4)$$

where: $\frac{dm_N}{dt}$ is the rate of mass transfer of nitrogen (kg.s$^{-1}$),

$A$ is the weld pool surface area (m$^2$),

$k$ is the reaction rate constant for reaction (5.1) (kg.m$^{-2}$.s$^{-1}$.atm$^{-1}$),

$N$(g) is the monatomic nitrogen content of the welding arc (atm),

$N_{eq}$(g) is the monatomic nitrogen content of the arc plasma required for equilibrium with the nitrogen in the steel (atm),

$N_{steel}$ is the weld metal nitrogen content (wt%),

$K$ is the apparent equilibrium constant for reaction (5.1),

$\rho$ is the density of the molten weld metal (kg.m$^{-3}$), and

$V$ is the volume of the molten weld pool (m$^3$).

(2) Nitrogen entering the weld pool as a result of nitrogen-containing base metal melting at the leading edge of the weld pool:

If the weld pool has a length $L$, the time required to melt a volume of metal equal to the volume of the weld pool is equal to $L/v$, where $v$ is the travel speed of the arc during welding. The melting rate of the base metal (in $kg.s^{-1}$) is therefore represented by equation (5.5).

$$\text{Melting rate} = \rho V\left(\frac{v}{L}\right) \qquad \ldots(5.5)$$

The rate of mass transfer of nitrogen from the base metal into the weld pool is then given by equation (5.6). Rewriting in terms of mass percentages yields equations (5.7) and (5.8):

$$\frac{dm_N}{dt} = \frac{N_i(wt\%)}{100}\rho V\left(\frac{v}{L}\right) \qquad \ldots(5.6)$$

$$\therefore \quad \frac{d(\%\underline{N})}{dt} = \frac{100}{\rho V}\frac{N_i(wt\%)}{100}\rho V\left(\frac{v}{L}\right) \qquad \ldots(5.7)$$

$$\therefore \quad \frac{d(\%\underline{N})}{dt} = N_i(wt\%)\left(\frac{v}{L}\right) \qquad \ldots(5.8)$$

where: $N_i$ is the initial nitrogen content of the base metal (wt%).

(3) Nitrogen leaving the weld pool by recombining to form $N_2$:

The evolution of nitrogen from the weld metal is represented by equation (5.9), and the rate of mass transfer for this reaction by the second order rate equations (5.10) and (5.11). Rewriting this expression in terms of mass percentages yields equation (5.12).

$$2\underline{N}\ (wt\%) \rightarrow N_2\ (g) \qquad \ldots(5.9)$$

$$\frac{dm_N}{dt} = -k'A({N_{steel}}^2 - {N_{eq}}^2) \qquad \ldots(5.10)$$

$$\therefore \quad \frac{dm_N}{dt} = -k'A({N_{steel}}^2 - K'P_{N_2}) \qquad \ldots(5.11)$$

$$\therefore \quad \frac{d(\%\underline{N})}{dt} = -\frac{100Ak'}{\rho V}[{N_{steel}}^2 - K'P_{N_2}] \qquad \ldots(5.12)$$

where: $k'$ is the reaction rate constant for reaction (5.9) ($kg.m^{-2}.s^{-1}.[\%N]^{-2}$),

$N_{eq}$ is the equilibrium nitrogen content of the molten metal at the weld pool temperature (wt%) for equilibrium with the nitrogen in the shielding gas,

$K'$ is the apparent equilibrium constant for the reaction: $N_2\,(g) \rightarrow 2\underline{N}$ (wt%), and

$P_{N_2}$ the nitrogen partial pressure in the shielding gas (atm).

(4) Nitrogen leaving the weld metal by resolidifying at the rear of the molten pool:

Since the solidification rate at the rear of the weld pool is equal to the melting rate (given by equation (5.5)), the rate at which nitrogen leaves the pool by resolidifying is represented by equation (5.13).

$$\frac{d(\%\underline{N})}{dt} = -N_{steel}\left(\frac{v}{L}\right) \qquad \ldots(5.13)$$

Assumption (c) listed above states that the amount of nitrogen entering the weld pool is equal to the amount of nitrogen leaving the weld pool per unit time under steady-state conditions. From the above, it follows that $N_{steel}$ must be equal to the steady-state nitrogen content, $N_{ss}$, and the total of equations (5.4) and (5.8) must be equal to the total of equations (5.12) and (5.13) under steady-state conditions:

$$\therefore \quad \frac{100Ak}{\rho V}\left[N(g)-\frac{N_{ss}}{K}\right]+N_i(wt\%)\left(\frac{v}{L}\right)=\frac{100Ak'}{\rho V}[N_{ss}{}^2-K'P_{N_2}]+N_{ss}\left(\frac{v}{L}\right) \qquad \ldots(5.14)$$

Rearranging equation (5.14) to collect all the terms containing the steady-state nitrogen content, $N_{ss}$ (wt%), on the left yields equation (5.15):

$$\frac{100Ak'}{\rho V}N_{ss}{}^2+\frac{v}{L}N_{ss}+\frac{100Ak}{\rho V}\frac{N_{ss}}{K}=\frac{100Ak'}{\rho V}K'P_{N_2}+\frac{100Ak}{\rho V}N(g)+\frac{v}{L}N_i(wt\%) \qquad \ldots(5.15)$$

For a specific shielding gas composition and set of welding parameters, the weld pool area, $A$, length, $L$, and volume, $V$, the monatomic nitrogen content of the arc, $N$(g), the welding speed, $v$, the density of the molten metal, $\rho$, the equilibrium constants, $K$ and $K'$, and the nitrogen partial pressure in the shielding gas, $P_{N_2}$, should remain constant, regardless of the base metal nitrogen content, $N_i$(wt%), and the surface active element concentration in the weld metal. The following conclusions can now be drawn from equation (5.15):

According to equation (5.15), the steady-state nitrogen content, $N_{ss}$(wt%), is dependent on the base metal nitrogen content, $N_i$(wt%), with an increase in the base metal nitrogen concentration leading to an increase in the steady-state nitrogen content. This has been observed experimentally, as shown in Figures 4.6 and 4.7. The extent of this dependence, however, is determined by the magnitude of the two reaction rate constants, $k$ (for the absorption reaction) and $k'$ (for the desorption reaction). Earlier results suggested that these rate constants vary with the surface active element concentration in the weld metal. In the low sulphur steels, desorption of nitrogen from the weld pool is rapid, leading to high values of $k'$, whereas desorption is retarded in the high sulphur alloys, resulting in low $k'$ values. The absorption rate constant, $k$, is not expected to be a strong function of the surface active element concentration. The values of the reaction rate constants for the experimental alloys will be determined in §5.2.5.

Due to the low desorption rate constant in the high sulphur alloys, equation (5.15) suggests that the steady-state nitrogen content is a strong function of the base metal nitrogen content, with $N_{ss}$(wt%) increasing as $N_i$(wt%) increases. This is consistent with the results shown in Figure 4.7. In the case of the low sulphur alloys, $k'$ is expected to be higher and gas-metal (or plasma-metal) reactions should therefore play a more significant role in determining the steady-state nitrogen content. According to equation (5.15), the influence of the base metal nitrogen content on the steady-state weld metal nitrogen level is less pronounced in the presence of high $k'$ values. This is consistent with the results shown in Figure 4.6.

## 5.2 VALUES OF THE CONSTANTS

In order to use equation (5.15) to predict the nitrogen content of the experimental alloys after welding, a number of constants, including the partial pressure of monatomic nitrogen in the arc, $N$(g), the weld pool surface area, $A$, volume, $V$, and length, $L$, the density of the molten metal, $\rho$, the two apparent equilibrium constants for the absorption and desorption reactions, $K$ and $K'$, and the two reaction rate constants, $k$ and $k'$, have to be determined. This section describes how the values of these constants were determined experimentally or calculated using relationships available in published literature.

### 5.2.1 Partial pressure of monatomic nitrogen in the arc plasma

The partial pressure of monatomic nitrogen in the arc plasma can be estimated using the method developed by Mundra and DebRoy[2] and Palmer and DebRoy[3] as part of the two-temperature model described in §1.4.1. These authors derived equation (5.17) for calculating the partial pressure of monatomic nitrogen formed as a result of the dissociation of molecular nitrogen, reaction (5.16), in the arc plasma:

$$\tfrac{1}{2}N_2\,(g) \rightarrow N\,(g) \qquad \ldots(5.16)$$

$$P_N = \sqrt{P_{N_2}}\exp\left(-\frac{\Delta G^0_{16,T_d}}{RT_d}\right) \qquad \ldots(5.17)$$

where: $P_N$ *is* the partial pressure of monatomic nitrogen in the arc plasma (atm),
$P_{N_2}$ is the partial pressure of diatomic nitrogen in the arc plasma (atm),
$\Delta G^0_{16,Td}$ is the standard free energy for reaction (5.16) at $T_d$,
$T_d$ is the effective dissociation temperature of diatomic nitrogen, and
$R$ is the universal gas constant (8,314 $J.K^{-1}.mol^{-1}$).

The extent of dissociation of diatomic nitrogen at $T_d$ can be calculated from equation (5.17) if the values of $P_{N_2}$, $T_d$ and $\Delta G^0_{16,Td}$ are known. Since the extent of dissociation of diatomic nitrogen is low under typical welding conditions, $P_{N_2}$ can be assumed to be equal to the partial pressure of $N_2$ in the inlet gas. The free energy of formation of monatomic nitrogen from diatomic $N_2$, $\Delta G^0_{16,Td}$, used by Mundra and DebRoy[2] and Palmer and DebRoy[3] (given by equation (5.18)) was obtained from the compilation by Elliott and Gleiser[4]. However, the data in this reference appears to be in error, specifically with regards to the heat of formation of N from $N_2$. Elliott and Gleiser quote a value of 358,0 kJ/mol (of N), whereas Kubaschewski *et al*[5] report 472,7 kJ/mol. The latter value agrees exactly with the bond strength of the diatomic molecule of 945,44 kJ/mol (of $N_2$)[6]. It therefore appears that the value given by Elliott and Gleiser is in error.

$$\Delta G^0_{16,T} = 86596 - 15{,}659T \qquad \text{(cal/mol)} \qquad \ldots(5.18)$$

One implication of this is that the conclusion of Palmer and DebRoy[3] that the effective plasma temperature (as regards the dissociation of $N_2$) is 100°C higher than the metal surface temperature, is in error, because this conclusion was based on the data of Elliott and Gleiser[4]. In the current work, this inaccuracy was corrected by recalculating the "effective dissociation temperature" as that temperature

which yields - for the conditions of the Palmer and DebRoy[3] experiments – the same partial pressure of monatomic nitrogen when the Kubaschewski *et al*[5] data are used, as does the Elliott and Gleiser data at a temperature of 1400°C, which is 100°C higher than the surface temperature in the Palmer and DebRoy investigation. This yields a reassessed effective plasma temperature of 1933°C, or 633°C higher than the surface temperature – much higher than the value reported by Palmer and DebRoy.

If the surface temperature of the weld pool is assumed to be approximately equal to the measured weld pool temperature of 1722°C, the values of $P_{N_2}$, $\Delta G^0_{16,Td}$, $T_d$ and $R$ can be substituted into equation (5.17), and the partial pressure of monatomic nitrogen in the arc plasma can be estimated for all the shielding gas atmospheres used in this investigation. The calculated monatomic nitrogen partial pressures are shown in Table 5.1, taking into consideration that total atmospheric pressure in Pretoria, where the experiments were performed, is 0,86 atm.

**Table 5.1** The estimated monatomic nitrogen partial pressure in the arc atmosphere as a function of the shielding gas nitrogen content for an effective plasma temperature of 2628 K.

| Shielding gas nitrogen content | Nitrogen partial pressure, $P_{N_2}$ | Monatomic nitrogen partial pressure, $P_N$ |
|---|---|---|
| 1,09 % | 0,0094 atm | $8{,}43.10^{-8}$ atm |
| 5,3 % | 0,0456 atm | $1{,}86.10^{-7}$ atm |
| 9,8 % | 0,0843 atm | $2{,}53.10^{-7}$ atm |
| 24,5 % | 0,2107 atm | $4{,}00.10^{-7}$ atm |

### 5.2.2 The weld pool surface area, *A*, length, *L*, and volume, *V*

The area and length of the weld pool were estimated by assuming that the crater at the end of each weld bead, where insufficient liquid metal was present to fill the depression created by the arc jet, has the same dimensions as the weld pool during welding. In order to determine these dimensions, the end craters of seven weld beads were photographed, and the resulting photographs enlarged. An example is shown in Figure 5.2. The maximum length of each crater was measured, taking into consideration the magnification, and the area was determined by superimposing the outline of the depression in each photograph on graph paper. The average values of the weld pool length and area determined using this method are shown in Table 5.2.

**Table 5.2** Weld pool dimensions.

| | |
|---|---|
| Weld pool surface area | $34{,}1 \pm 4{,}8$ mm$^2$ |
| Weld pool length | $7{,}4 \pm 0{,}5$ mm |
| Weld pool volume | $63{,}9 \pm 6{,}3$ mm$^3$ |

The volume of the weld pool was estimated by sectioning two weld beads and photographing polished and etched cross sections. An example of such a photograph is shown in Figure 5.3. If it is assumed that the weld pool has the shape of a section of a sphere, equation (5.19) can be used to calculate the weld pool volume[7].

**Figure 5.2** The end crater of a weld bead. Magnification: 10x.

**Figure 5.3** A cross section of a weld bead. Magnification: 10x.

$$V = \frac{1}{3}\pi r^3(2 - 3\cos\theta + \cos^3\theta) \qquad \ldots(5.19)$$

where: $r$ is the radius of the sphere, and

$\theta$ is the angle between the fusion line and the plate at the surface of the sample.

The average weld pool volume is shown in Table 5.2.

### 5.2.3 The apparent equilibrium constants, *K* and *K'*

- The apparent equilibrium constant for the desorption reaction, *K'*

If nitrogen desorption from the weld pool during welding is represented by equation (5.9), the apparent equilibrium constant, *K'*, for this reaction is given by equation (5.20).

$$K' = \frac{[N_{eq}(wt\%)]^2}{P_{N_2}} \qquad \ldots(5.20)$$

As described in §1.2.3, the equilibrium nitrogen content as a function of temperature can be calculated using equation (5.21)[8].

$$\log(\underline{N_{eq}}) = -\frac{247}{T} - 1{,}22 - \left(\frac{4780}{T} - 1{,}51\right)\log f_{N,1873} - \left(\frac{1760}{T} - 0{,}91\right)(\log f_{N,1873})^2 \qquad \ldots(5.21)$$

where: $T$ is the temperature (K), and

$f_{N,1873}$ is the nitrogen activity coefficient $f_N$ at 1873 K.

The activity coefficient, $f_N$, that is required for substitution in equation (5.21) can be calculated from the chemical composition of the steel using equation (5.22).

$$\begin{aligned}\log f_N = \{&-164[\%Cr] + 8{,}33[\%Ni] - 33{,}2[\%Mo] - 134[\%Mn] + 1{,}68[\%Cr]^2 - 1{,}83[\%Ni]^2 \\ &- 2{,}78[\%Mo]^2 + 8{,}82[\%Mn]^2 + (1{,}6[\%Ni] + 1{,}2[\%Mo] + 2{,}16[\%Mn]).[\%Cr] + \\ &(-0{,}26[\%Mo] + 0{,}09[\%Mn]).[\%Ni]\}/T + \{0{,}0415[\%Cr] + 0{,}0019[\%Ni] + \\ &0{,}0064[\%Mo] + 0{,}035[\%Mn] - 0{,}0006[\%Cr]^2 + 0{,}001[\%Ni]^2 + 0{,}0013[\%Mo]^2 - \\ &0{,}0056[\%Mn]^2 + (-0{,}0009[\%Ni] - 0{,}0005[\%Mo] - 0{,}0005[\%Mn]).[\%Cr] + \\ &(0{,}0003[\%Mo] + 0{,}0007[\%Mn]).[\%Ni]\} + 0{,}13[\%C] + 0{,}06[\%Si] + 0{,}046[\%P] \\ &+ 0{,}007[\%S] + 0{,}01[\%Al] - 0{,}9[\%Ti] - 0{,}1[\%V] - 0{,}003[\%W] - 0{,}12[\%O]\end{aligned} \qquad \ldots(5.22)$$

where: [%M] is the alloying element content in wt%.

Calculation yields the equilibrium nitrogen contents shown in Table 5.3 at a weld pool temperature of 1722°C, taking into consideration that total atmospheric pressure in Pretoria is 0,86 atm. These values were substituted into equation (5.20) to yield an average apparent equilibrium constant of $4{,}28.10^{-2}$ for the nitrogen desorption reaction.

**Table 5.3** The equilibrium nitrogen content of the weld metal at the temperature of the centre of the pool (1722°C) as a function of the partial pressure of nitrogen in the shielding gas.

| Shielding gas nitrogen content | Nitrogen partial pressure, $P_{N_2}$ | Equilibrium nitrogen content, $N_{eq}$ |
|---|---|---|
| 1,09 % | 0,0094 atm | 0,0200 wt% |
| 5,3 % | 0,0456 atm | 0,0442 wt% |
| 9,8 % | 0,0843 atm | 0,0601 wt% |
| 24,5 % | 0,2107 atm | 0,0950 wt% |

- The apparent equilibrium constant for the absorption reaction, $K$

If the dissolution of monatomic nitrogen into the weld pool during welding is represented by equation (5.1), the apparent equilibrium constant, $K$, for this reaction is given by equation (5.23). In order to calculate the value of $K$, the relationship between $K$, $K'$ (the apparent equilibrium constant for the desorption of nitrogen) and $K_1$ (the equilibrium constant for the dissociation of molecular nitrogen to form

monatomic nitrogen in the arc) must be established. This relationship is shown in equation (5.24) with the equilibrium constant, $K_1$, for nitrogen dissociation (reaction (5.16)) given by equation (5.25).

$$K = \frac{N_{eq}}{P_N} \qquad \ldots(5.23)$$

where: $N_{eq}$ is the nitrogen concentration in the steel in equilibrium with the monatomic nitrogen content of the arc plasma.

$$K = \frac{\sqrt{K'}}{K_1} \qquad \ldots(5.24)$$

where: $$K_1 = \frac{P_N}{\sqrt{P_{N_2}}} \qquad \ldots(5.25)$$

Since the partial pressure of molecular nitrogen in the arc, $P_{N_2}$, and the value of the equilibrium constant for the nitrogen desorption reaction, $K'$, are known (refer to §5.2.3), and the partial pressure of monatomic nitrogen in the arc plasma at the weld pool temperature can be determined, the apparent equilibrium constant for the absorption of monatomic nitrogen, $K$, can be calculated. Calculation yields an average $K$ value of $2{,}55.10^8$ at the weld pool temperature of 1722°C.

### 5.2.4 Density of the molten weld pool

The densities of liquid iron, nickel, chromium and manganese as linear functions of temperature, $T$, in °C can be calculated using equations (5.26) to (5.29)[9], where $T$ is the temperature of the centre of the weld pool in°C.

| | | |
|---|---|---|
| Iron: | $8{,}30 - 8{,}36.10^{-4}T$ | …(5.26) |
| Nickel: | $9{,}60 - 12{,}00.10^{-4}T$ | …(5.27) |
| Chromium: | $7{,}83 - 7{,}23.10^{-4}T$ | …(5.28) |
| Manganese: | $7{,}17 - 9{,}30.10^{-4}T$ | …(5.29) |

This method yields a density of 6,755 g.cm$^{-3}$ or 6755 kg.m$^{-3}$ for the experimental type 310 alloys used in this investigation.

### 5.2.5 The nitrogen desorption and absorption rate constants, *k'* and *k*

- The nitrogen desorption rate constant, *k'*

Correlations based on the rate of reaction of molecular nitrogen with pure iron were used to estimate the rate constant for the loss of nitrogen from the weld pool as $N_2$ (reaction (5.9)). The available data on this rate constant were summarised by Belton[10] and Turkdogan[11]. For the reaction $N_2$ (g) → 2N (wt%), the rate constant (for temperatures ranging from 1550 to 1700°C) is given by equation (5.30):

$$k_1 = \frac{10^{(-6340/T+1{,}85)}}{1+260 f_O[\%O]+130 f_S[\%S]} \quad \text{g.cm}^{-2}.\text{min}^{-1}.\text{atm}^{-1} \qquad \ldots(5.30)$$

where: $T$ is the temperature in K,

$f_O$ is the activity coefficient of dissolved oxygen,

[%O] is the mass percentage of dissolved oxygen,

$f_S$ is the activity coefficient of dissolved sulphur, and

[%S] is the mass percentage of dissolved sulphur.

The rate expression used with this rate constant is as follows:

$$\frac{d\underline{N}(\text{wt\%})}{dt} = \frac{100A}{\rho V} k_1 \left[ P_{N_2} - \frac{[\text{N(wt\%)}]^2}{K'} \right] \qquad \ldots(5.31)$$

This expression can be rewritten as:

$$\frac{d\underline{N}(wt\%)}{dt} = -\frac{100A}{\rho V} \frac{k_1}{K'} \left[ [N(wt\%)]^2 - K' P_{N_2} \right] \qquad \ldots(5.32)$$

Equation (5.32) can be seen to be the same expression as equation (5.12), with $k' = k_1/K'$.

For stainless steels, the rate constant for this reaction is generally larger than that for liquid iron by a factor of about 6[10,12]. However, this conclusion is based on experiments conducted at 1600°C, and (as will be shown later) it appears that increasing the rate constant by this factor leads to an overestimate.

For stainless steels, the activity coefficient of sulphur, $f_S$, can be estimated as follows[13]:

$$\log f_S = [\%\text{Cr}] \left( -\frac{94{,}2}{T} + 0{,}040 \right) \qquad \ldots(5.33)$$

where: $T$ is the absolute temperature, and

[%Cr] is the mass percentage of chromium in the steel.

For a weld pool temperature of 1722°C and an average chromium content of 24,4%, this yields a value of $f_S = 0{,}67$.

In these calculations, the effect of dissolved oxygen on the rate constant was neglected, since no data were available on the oxygen levels. However, the activity of oxygen is expected to be low in chromium-rich steels, and since the sulphur levels are comparatively high, neglecting the effect of dissolved oxygen is not expected to affect the calculations significantly.

Substitution of the constants and unit conversion yield the following expression for the rate constant, for a temperature of 1722°C:

$$k' = \frac{0{,}183}{1 + 87[\%\text{S}]} \quad \text{kg.m}^{-2}.\text{s}^{-1}.(\%)^{-2} \qquad \ldots(5.34)$$

This value of the desorption rate constant is for liquid iron, not for stainless steel. However, it appears that it better predicts the rate of the formation of molecular nitrogen than if the rate constant is increased by a factor of 6, which has been suggested to be appropriate for stainless steels[10]. Part of the reason for choosing not to increase the rate constant over that for pure iron is illustrated in Figure 5.4 below, which

compares the measured and predicted reduction in the weld nitrogen content, for welding under pure argon. When welding in pure argon, no dissociated (monatomic) nitrogen is assumed to form in the plasma, and hence the (unknown) rate constant $k$ (for the reaction $N_{plasma} \rightarrow [\underline{N}]_{steel}$) has no effect on the weld nitrogen content which is calculated with equation (5.15). As the figure shows, both values of the rate constant $k'$ overpredict the decrease in nitrogen content of the weld, but the correspondence is much better for the smaller rate constant.

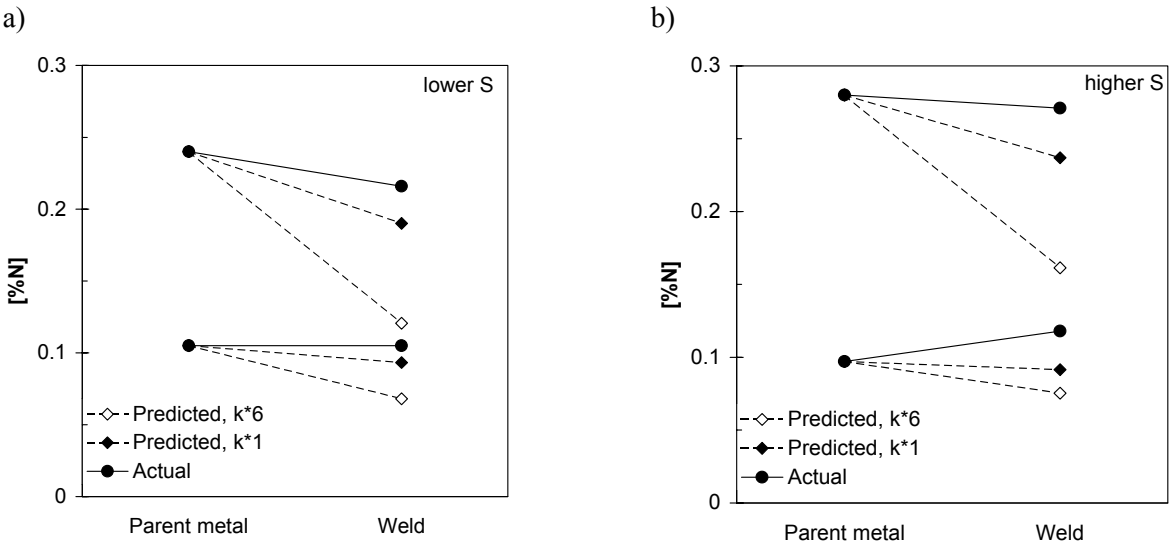


**Figure 5.4** Comparison of the actual decrease in nitrogen content from the original parent metal composition (filled circles), with the calculated decrease using the rate constant for liquid iron (filled diamonds), and for the case where this rate constant is increased by a factor of 6 (open diamonds). Results are shown for a) the low sulphur and b) the high sulphur steels, in both cases for welding in pure argon.

Based on these conclusions, equation (5.34) yields values for the desorption rate constant, $k'$, of $6{,}28.10^{-2}$ and $3{,}21.10^{-2}$ $kg.m^{-2}.s^{-1}.(\%)^{-2}$ for the low and high sulphur alloys, respectively. The reduction in the desorption rate constant at higher surface active element concentrations is consistent with a site blockage model, where sulphur atoms are assumed to occupy a fraction of the surface sites required for the adsorption of nitrogen.

- The nitrogen absorption rate constant, $k$

Literature data on the value of the rate constant $k$ for the reaction of dissociated (monatomic) nitrogen with the stainless steel melt are very limited. For this reason, this constant was estimated from the experimental data, for the case where the shielding gas contained 1,09% nitrogen. These data were used, since nitrogen bubbles formed in the weld pool at higher nitrogen contents. Formation of nitrogen bubbles render one of the assumptions on which the model is based, invalid. Calculated values of the absorption rate constant are summarised in Table 5.4 below.

As the table shows, use of the larger rate constant $k'$ yields values for the constant $k$ which appear to depend on the initial nitrogen content of the steel. There appears to be no fundamental reason why this should be the case. When the rate constant $k'$ for liquid iron is used in its original form, the rate constant

$k$ is approximately the same for all the steels. Interestingly, no strong effect of the sulphur content on the rate constant for dissociated nitrogen is found. This is in contrast with the case for the reaction which involves molecular nitrogen, where an increase in sulphur from 0,022% to 0,054% causes a decrease in the rate constant $k'$ by a factor of approximately 2. Given the weak dependence of $k$ on steel composition, an average value of $3{,}5.10^4$ $kg.m^{-2}.s^{-1}.atm^{-1}$ was used in the subsequent calculations (together with the value of $k'$ as for liquid iron).

**Table 5.4** Calculated values of the rate constant $k$ for the absorption of dissociated nitrogen by the weld pool.

a) Rate constant $k'$ for liquid iron.

| Alloy | Comments | Base metal nitrogen content | Sulphur content | $10^{-3}k$ ($kg.m^{-2}.s^{-1}.atm^{-1}$) |
|---|---|---|---|---|
| VFA 657 | Low N, low S | 0,005 | 0,023 | 38 |
| VFA 658 | Medium N, low S | 0,105 | 0,023 | 43 |
| VFA 659 | High N, low S | 0,240 | 0,022 | 35 |
| VFA 752 | Low N, high S | 0,006 | 0,052 | 36 |
| VFA 753 | Medium N, high S | 0,097 | 0,061 | 30 |
| VFA 755 | High N, high S | 0,280 | 0,049 | 27 |

b) Rate constant $k'$ taken to be 6 times that for liquid iron.

| Alloy | Comments | Base metal nitrogen content | Sulphur content | $10^{-3}k$ ($kg.m^{-2}.s^{-1}.atm^{-1}$) |
|---|---|---|---|---|
| VFA 657 | Low N, low S | 0,005 | 0,023 | 57 |
| VFA 658 | Medium N, low S | 0,105 | 0,023 | 124 |
| VFA 659 | High N, low S | 0,240 | 0,022 | 210 |
| VFA 752 | Low N, high S | 0,006 | 0,052 | 46 |
| VFA 753 | Medium N, high S | 0,097 | 0,061 | 61 |
| VFA 755 | High N, high S | 0,280 | 0,049 | 159 |

### 5.2.6 Summary of the constants required in equation (5.15)

A summary of all the constants required for substitution into equation (5.15) is given in Table 5.5.

## 5.3 PREDICTED CHANGE IN THE WELD METAL NITROGEN CONCENTRATION WITH INCREASING SHIELDING GAS NITROGEN CONTENT

Figure 5.5 below shows the predicted change in weld nitrogen content, for shielding gases with increasing nitrogen content. The calculations were performed for parent metal with the same composition as the experimental alloys. It can be seen that the predicted behaviour is close to that found experimentally (Figures 4.6 and 4.7), with marked increases in the weld nitrogen content at low shielding gas nitrogen

contents. The influence of the base metal nitrogen content and the surface active element concentration on the weld metal nitrogen content is also consistent with that observed experimentally.

**Table 5.5** Summary of the constants required in equation (5.15).

| Constant | Value |
|---|---|
| $P_N$ | $8{,}43.10^{-8}$ atm if $P_{N_2}$ = 0,0094 atm<br>$1{,}86.10^{-7}$ atm if $P_{N_2}$ = 0,0456 atm<br>$2{,}53.10^{-7}$ atm if $P_{N_2}$ = 0,0843 atm<br>$4{,}00.10^{-7}$ atm if $P_{N_2}$ = 0,2107 atm |
| $A$ | 34,1 $mm^2$ |
| $L$ | 7,4 mm |
| $V$ | 63,9 $mm^3$ |
| $K$ | $2{,}55.10^{8}$ |
| $K'$ | $4{,}28.10^{-2}$ |
| $\rho$ | 6755 $kg.m^{-3}$ |
| $v$ | 2,7 $mm.s^{-1}$ |
| $k$ | $3{,}5.10^{4}$ $kg.m^{-2}.s^{-1}.atm^{-1}$ |
| $k'$ | $6{,}28.10^{-2}$ $kg.m^{-2}.s^{-1}.(\%)^{-2}$ for the low sulphur alloys<br>$3{,}21.10^{-2}$ $kg.m^{-2}.s^{-1}.(\%)^{-2}$ for the high sulphur alloys |

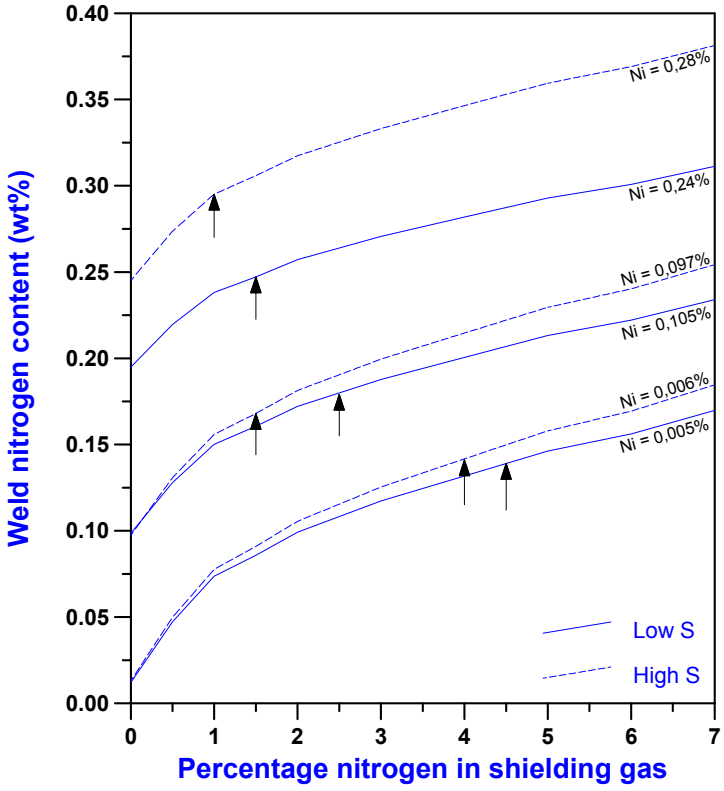


**Figure 5.5** Predicted change in weld nitrogen content for shielding gases which are increasingly rich in nitrogen. Calculated for the parent metal compositions of the experimental alloys. The arrows indicate the minimum shielding gas compositions where bubbling was observed experimentally.

The results shown in Figure 5.5 are only valid until the onset of bubble formation. The shielding gas compositions where bubbling was observed visually are indicated on this figure. Beyond this point, nitrogen is removed from the weld pool not only by the gas-metal reaction at the weld pool surface, but also by bubble formation within the weld pool. This condition is not covered by the simple kinetic model presented here. For shielding gas compositions at the onset of bubbling, the predicted rates at which nitrogen enters and leaves the welding pool by the four mechanisms considered in the model are summarised in Table 5.6. This shows that the main mechanism by which nitrogen enters the weld pool is a function of the initial nitrogen content of the alloy, with nitrogen absorption from the arc plasma playing a dominant role at low base metal nitrogen contents, and the melting of nitrogen-containing base metal at high initial nitrogen levels. The main exit mechanism appears to be nitrogen leaving the pool due to the solidification of nitrogen-containing weld metal at the rear of the weld pool, rather than nitrogen desorption to the atmosphere as $N_2$. It is evident from Figure 5.6 that higher concentrations of sulphur in the weld pool slightly retard the desorption of $N_2$ to the atmosphere (giving higher nitrogen contents in the weld pool for a similar base metal nitrogen content). This is consistent with a site blockage model, where sulphur atoms occupy a fraction of the surface sites required for the adsorption of nitrogen.

**Table 5.6** The relative contributions of the four reactions which add or remove nitrogen to or from the weld pool, at the respective shielding gas compositions where bubble formation was observed experimentally.

| | | $\frac{dN(wt\%)}{dt}$, mg.s$^{-1}$ | | | |
|---|---|---|---|---|---|
| **Alloy** | **Comments** | **(1) Absorption of monatomic N from plasma** | **(2) Melting of base metal at leading edge of weld pool** | **(3) Desorption of $N_2$ from the weld pool** | **(4) Solidification at the rear of the weld pool** |
| VFA 657 | Low N, low S | 0,203 | 0,008 | -0,025 | -0,185 |
| VFA 658 | Medium N, low S | 0,151 | 0,165 | -0,055 | -0,261 |
| VFA 659 | High N, low S | 0,116 | 0,378 | -0,120 | -0,374 |
| VFA 752 | Low N, high S | 0,191 | 0,009 | -0,014 | -0,187 |
| VFA 753 | Medium N, high S | 0,117 | 0,153 | -0,024 | -0,246 |
| VFA 755 | High N, high S | 0,095 | 0,441 | -0,093 | -0,442 |

Two factors are of interest in the practical welding situation: the change in nitrogen content upon welding, and the formation of nitrogen bubbles. The former situation appears to be fairly well described by the kinetic model presented here. However, the latter is more difficult to predict. As Figures 4.6 and 4.7 show, bubble formation was observed for weld nitrogen contents ranging from 0,16% to 0,29%. In comparison, the equilibrium nitrogen content for a nitrogen partial pressure of 0,86 atm (atmospheric pressure in Pretoria) is 0,19% at 1722°C. (The saturation concentration depends somewhat on temperature, as shown in Figure 5.6 for the experimental alloys).

For the formation of a nitrogen bubble in the weld pool, the nitrogen partial pressure within the bubble must at least equal atmospheric pressure (in fact, it must be slightly larger than atmospheric pressure to

balance the surface tension of the bubble). Considering that the nitrogen saturation content at 0,86 atm is 0,19%, the high nitrogen alloys display a significant degree of supersaturation prior to the onset of bubble formation (as shown in Figure 5.5). This is consistent with the results of Blake and Jordan[14], who reported that the steady-state nitrogen content of molten iron is in excess of that required to provide an internal pressure of one atmosphere at the assumed temperature of the liquid metal, and concluded that some degree of supersaturation occurs. The increased levels of supersaturation for the higher-nitrogen alloys are presumably related to the higher rate of nitrogen removal as $N_2$ at the onset of bubble formation; this higher rate of $N_2$ formation is evident from Table 5.6. Given that nitrogen bubble formation and detachment require bubble nucleation and growth, it appears reasonable to assume that a higher nitrogen removal rate (as bubbles) would require a higher degree of supersaturation (a larger "driving force" for the reaction). Such a link between supersaturation and the rate of nitrogen removal is also evident in the experimental results shown in Figures 4.6 and 4.7, where the weld metal nitrogen concentration increases if the shielding gas nitrogen content is increased beyond the onset of bubble formation.

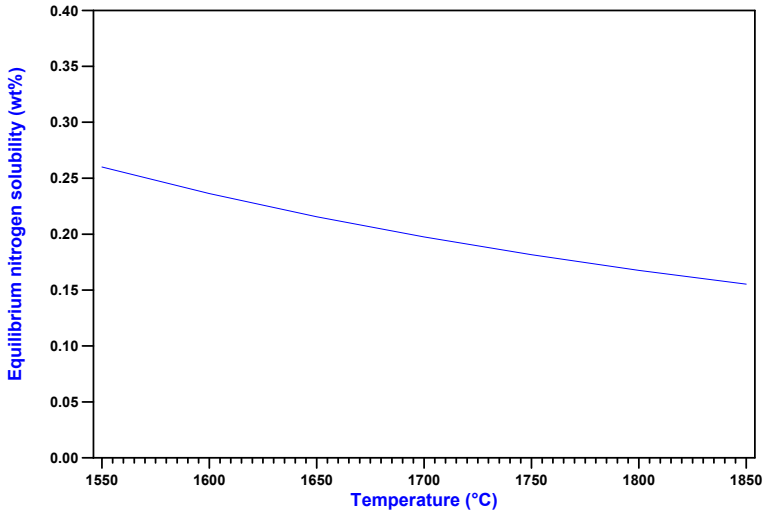


**Figure 5.6** The influence of weld pool temperature on the equilibrium nitrogen concentration in the experimental alloys at a nitrogen partial pressure of 0,86 atm. (Calculated using Wada and Pehlke's equations and interaction parameters[8]).

On the other hand, it does not appear possible to form bubbles at weld nitrogen contents below 0,19%, as was found experimentally for most of the lower nitrogen alloys. Possible reasons for this discrepancy include deviation of the (average) weld pool temperature from that measured, deviation of the actual saturation concentration of nitrogen from that predicted by the correlation for $f_N$, and errors in chemical analysis. Some of these factors are briefly considered below.

As shown in Figure 5.6, a change in temperature has a limited influence on the equilibrium nitrogen concentration of the experimental steels at 0,86 atm. A variation in the weld pool temperature from that measured during the course of this investigation is therefore not expected to have a significant influence

on the equilibrium solubility at 0,86 atm. Experimental error in chemical analysis may, however, be largely responsible for the discrepancy described above. In order for inert gas fusion analysis for nitrogen to be as accurate as possible, weld metal drillings have to be removed very carefully to prevent base metal contamination. Since the weld pools formed during this investigation were relatively shallow, a limited amount of contamination may have occurred. This will influence the nitrogen contents associated with the onset of bubble formation in the experimental alloys. An additional complicating factor is that the minimum shielding gas nitrogen content required to initiate bubbling in each of the experimental alloys (as shown by the arrows in Figure 5.5) was determined by visually observing the weld pool during welding. The transition from nitrogen evolution at the weld pool surface to bubble formation is gradual, making it difficult to accurately ascertain the minimum shielding gas nitrogen level required to initiate bubbling. It is therefore debatable whether any deviation of the measured nitrogen content at the onset of bubble formation from the equilibrium solubility at 0,86 atm is significant.

## 5.4 THE INFLUENCE OF THE SURFACE ACTIVE ELEMENT CONCENTRATION ON THE PREDICTED WELD NITROGEN CONTENT

Since it has been shown that the rate constant for the nitrogen absorption reaction, $k$, is only weakly dependent on the steel composition, and the influence of the sulphur concentration on the desorption rate constant, $k'$, can be calculated using equation (5.34), the kinetic model can be used to quantify the influence of the surface active element concentration, and in particular the sulphur content, on the weld nitrogen content. As stated earlier, the effect of dissolved oxygen on the rate constants can be neglected, since the activity of oxygen is expected to be low in chromium-rich steels. The influence of the sulphur concentration in the experimental steels on the predicted steady-state nitrogen content for a shielding gas nitrogen content of 1,09% is shown in Figure 5.7.

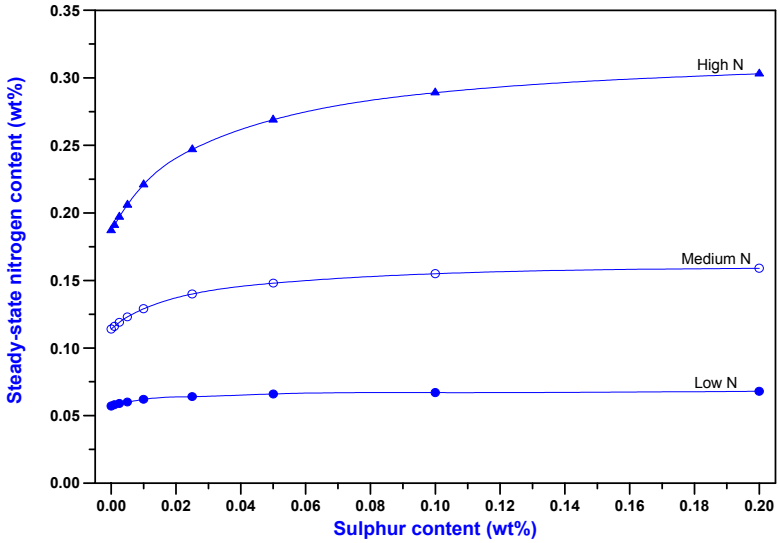


**Figure 5.7** The steady-state nitrogen content of the experimental steels as a function of sulphur content at a shielding gas nitrogen content of 1,09%.

Figure 5.7 shows that the steady-state nitrogen content initially increases and then approaches a constant value as the sulphur content increases. The decrease in the steady-state nitrogen content at low sulphur concentrations can be attributed to an increase in the desorption rate constant, $k'$, as demonstrated by equation (5.34). As a result of the lower level of surface coverage at low sulphur concentrations, more nitrogen can escape to the atmosphere during welding, resulting in higher nitrogen desorption rates and lower weld nitrogen contents. As the sulphur content increases, the desorption rate is reduced due to increased site blockage. Since the rate of nitrogen desorption is small in the experimental alloys (refer to Table 5.6), a further increase in sulphur content will have a limited influence on the total reaction rate, and the weld nitrogen content becomes independent of the surface active element concentration. The steady-state nitrogen content in the presence of surface active elements also appears to be a strong function of the base metal nitrogen content, which is consistent with the influence of the surface active element content on the desorption rate constant. In the presence of high levels of sulphur, the nitrogen desorption rate decreases and more of the nitrogen originally present in the base metal remains in solution in the weld metal. Higher base metal nitrogen contents therefore lead to higher weld nitrogen concentrations. This is consistent with the results shown in Figure 4.7 for the high sulphur alloys.

## 5.5 THE INFLUENCE OF WELDING PARAMETERS ON THE PREDICTED WELD NITROGEN CONCENTRATION

Several researchers have reported that welding parameters, in particular the welding current, arc voltage and torch travel speed, have a significant influence on nitrogen absorption and desorption during welding. The results of some of these investigations were described in §1.6. The potential impact of a change in welding parameters on the weld nitrogen content calculated using the kinetic model, is considered below.

According to Kuwana and Kokawa[15] and Kuwana *et al*[16], an increase in welding current reduces the weld metal nitrogen content. Since it has been shown that the welding current does not have a significant influence on the temperature of the weld pool, its effect on the weld nitrogen content appears to be related to a change in the weld pool dimensions. The weld pool surface area, volume and length are all expected to increase with an increase in welding current. The weld pool dimensions are also influenced by a change in the arc voltage and torch travel speed. The weld cross-sectional area initially increases with an increase in arc length (and therefore arc voltage), but becomes constant at higher arc lengths, whereas the weld pool area decreases markedly with an increase in travel speed.

Since an investigation into the influence of welding parameters on the dimensions of the weld pool falls outside the scope of this study, an attempt will be made to show how an arbitrary increase in the weld pool surface area, either as a result of an increase in welding current or arc voltage, or a decrease in torch travel speed, influences the steady-state nitrogen content predicted by the kinetic model.

If it is assumed that the weld pool has the shape of a section of a sphere (as shown schematically in Figure 5.8), equations (5.19) and (5.35) can be used to determine how an arbitrary change in weld pool surface area impacts on the weld pool volume and length. If, for example, a change in welding parameters causes the weld pool surface area to double in size from 34,1 $mm^2$ (refer to Table 5.2) to 68,2 $mm^2$, the weld

pool length, $L$, is expected to change from 7,4 mm to 9,6 mm, and the volume, $V$, from 63,9 mm$^3$ to 151,7 mm$^3$. These values can now be substituted into equation (5.15) to calculate the steady-state nitrogen content for the new set of welding parameters.

$$A = \pi r^2 \sin \theta \qquad \ldots(5.35)$$

where: $A$ is the area of a section of a sphere, where the sphere has a radius, $r$.

The weld nitrogen contents of two experimental alloys, VFA 657 and VFA 755 (i.e. the low N, low S and high N, high S steels) were calculated for the adjusted weld pool dimensions and are shown in Figure 5.9 as a function of the shielding gas nitrogen content. It is evident from this figure that a change in the weld pool dimensions as a result of a change in welding parameters does not cause a significant variation in the predicted weld nitrogen content.

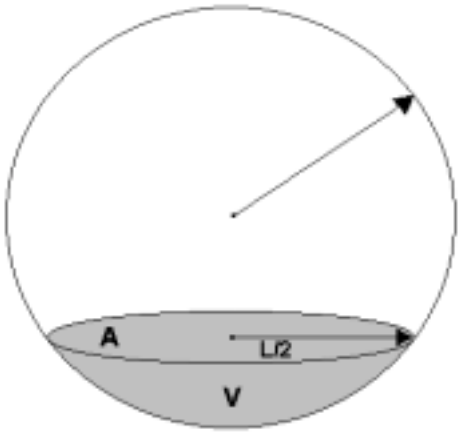


**Figure 5.8** The weld pool as a section of a sphere with radius, $r$. $A$ is the area of the circular section, $V$ is the volume of the section, and $L$ is the diameter of the circular section (as shown above).

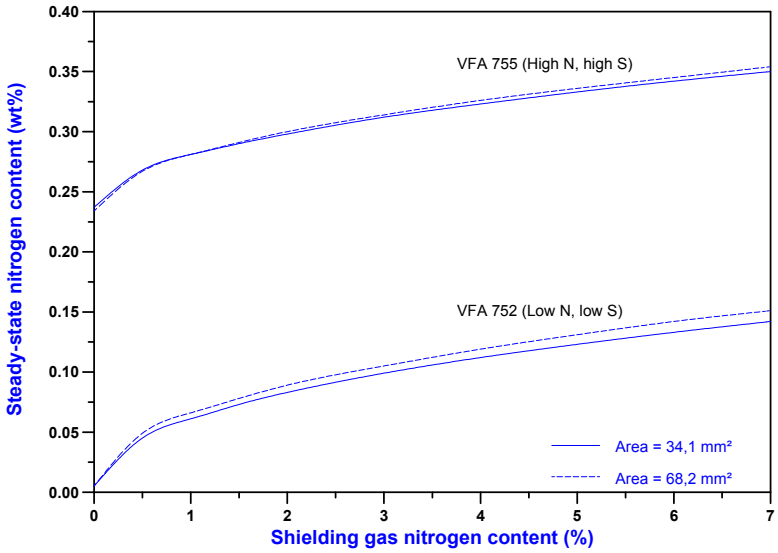


**Figure 5.9** The influence of a change in the weld pool dimensions on the steady-state nitrogen content of two experimental alloys.

A number of factors not considered in this approach may influence the calculated steady-state nitrogen content. These factors are listed below.

- As the torch travel speed increases during welding, the weld pool shape changes from circular or oval to teardrop shaped. When this happens, the assumption that the weld pool has the shape of a section of a sphere is no longer acceptable, and the ratio of the weld pool length, $L$, to the weld pool surface area, $A$, will increase. Since, according to the kinetic model, the weld pool length affects the rate at which nitrogen enters the weld pool due to melting and the rate at which nitrogen leaves the weld metal due to solidification, and these effects are important in determining the overall reaction rate, this change in weld pool shape is expected to have a significant influence on the predicted steady-state nitrogen content.

- Kuwana *et al*[15] suggested that, in the presence of pure nitrogen shielding gas, the nitrogen content of the weld metal may be controlled mainly by nitrogen evolution during cooling. According to these authors, an increase in the weld cross-sectional area results in a decrease in the cooling rate after welding, thereby prolonging the period of time before solidification and resulting in an increase in the amount of evolved nitrogen. Since a change in cooling rate after welding is not considered by the kinetic model, this may result in slightly lower nitrogen levels than those predicted.

- A change in welding parameters may change the extent of coverage of the weld pool by the arc plasma. Since full coverage of the weld pool by the arc was assumed on deriving the kinetic model, this is likely to impact on its predictions. Complete coverage of the weld pool by the plasma can be assumed if welding is performed at reasonably low currents and the weld pool is fairly narrow. Since nitrogen absorption only occurs under the plasma impingement area, whereas nitrogen desorption takes place over the entire weld pool surface area, incomplete coverage of the weld pool by plasma is expected to increase the desorption rate, resulting in lower steady-state nitrogen contents.

- Excessive arc lengths during welding will increase the likelihood of atmospheric contamination as more nitrogen from the surrounding atmosphere (air) is entrained in the arc plasma. This will change the nitrogen content of the arc and result in variations in the values of $P_N$ and $P_{N_2}$ from those expected based on the shielding gas nitrogen content.

## 5.6 CONCLUSIONS

- A kinetic model can be used to describe nitrogen absorption and desorption during the welding of the experimental stainless steels. The proposed model considers the absorption of monatomic nitrogen from the arc plasma, the evolution of $N_2$ from the weld pool, nitrogen entering the weld metal during the melting of nitrogen-containing base metal, and nitrogen leaving the weld pool due to the solidification of weld metal at the rear of the pool. The predictions of the model show good agreement with the experimental results discussed in Chapter 4.

- The calculated nitrogen desorption rate constant is a function of the surface active element concentration in the alloy, with the rate constant decreasing at higher concentrations of sulphur in the steel. This is consistent with a site blockage model, where surface active elements occupy a fraction of the surface sites required for nitrogen adsorption. The rate constant for the absorption of dissociated nitrogen is, however, not a strong function of the surface active element concentration.

- Nitrogen desorption rates are significantly lower in the presence of higher concentrations of surface active elements. The main mechanism by which nitrogen enters the weld pool is dependent on the initial nitrogen content of the alloy, with nitrogen absorption from the arc plasma playing a dominant role at low base metal nitrogen contents, and the melting of nitrogen-containing base metal at high initial nitrogen levels. The main exit mechanism appears to be nitrogen leaving the pool due to the solidification of nitrogen-containing weld metal at the rear of the weld pool, rather than nitrogen desorption to the atmosphere as $N_2$.

- Although the minimum shielding gas nitrogen content that leads to bubbling cannot be determined from the model, it is evident that some supersaturation above that required to nucleate nitrogen bubbles in the melt occurs in the high nitrogen alloys. This can probably be attributed to the higher rate of nitrogen removal as $N_2$ at the onset of bubble formation.

- A change in welding parameters does not appear to influence the steady-state nitrogen content in the experimental alloys to any significant extent.

## 5.7 PRACTICAL IMPLICATIONS

The results of the current investigation show that nitrogen losses from nitrogen-alloyed stainless steels can be expected during autogenous welding in pure argon shielding gas. In the experimental alloys this effect was most pronounced at base metal nitrogen contents in excess of 0,1%. Small amounts of nitrogen can be added to the shielding gas to counteract this effect, but this should be done with care to avoid bubble formation. However, supersaturation before bubble formation does extend the range of shielding gas compositions which can be used.

Higher concentrations of surface active elements have a beneficial influence on the behaviour of high nitrogen stainless steels during welding. Due to the lower desorption rates associated with higher surface active element concentrations, more of the base metal nitrogen originally present in the alloy will be maintained in solution in the weld pool. Higher sulphur contents also increase the steady-state nitrogen content of stainless steels and the amount of nitrogen that can be accommodated in the weld metal prior to nitrogen evolution in the form of bubbles. Although higher sulphur contents may not be viable in practice, small amounts of oxygen added to the shielding gas during welding will have a similar effect.

## 5.8 REFERENCES


1. T. Kuwana, H. Kokawa, and M. Saotome, "Quantitative prediction of nitrogen absorption by steel during gas tungsten arc welding". 3rd International Seminar on the Numerical Analysis of Weldability. Graz-Seggau, Austria. 25-27 September 1995.
2. K. Mundra, and T. DebRoy, "A general model for partitioning of gases between a metal and its plasma environment", Metallurgical and Materials Transactions B, vol. 26B. February 1995. pp. 149-157.
3. T.A. Palmer, and T. DebRoy, "Physical modeling of nitrogen partition between the weld metal and its plasma environment". Welding Journal, vol. 75, no. 7. July 1996. pp. 197s-207s.
4. J.F. Elliott, and M. Gleiser, "Thermochemistry for Steelmaking I". Addison-Wesley Publishing Company, Reading, USA. 1963. p. 75.
5. O. Kubaschewski, C.B. Alcock, and P.J. Spencer, "Materials Thermochemistry", 6th Edition. Pergamon, Oxford. 1993.
6. R.C. Weast, "CRC Handbook of Chemistry and Physics", 62nd Edition. CRC Press, Boca Raton, Florida. 1981.
7. R.E. Reed-Hill, and R. Abbaschian, “Physical Metallurgy Principles”, 3rd Edition. PWS Kent, Boston, USA. 1992. p. 497.
8. H. Wada, and R.D. Pehlke, "Solubility of nitrogen in liquid Fe-Cr-Ni alloys containing manganese and molybdenum". Metallurgical Transactions B, vol. 8B. December 1977. pp. 675-682.
9. R.J. Fruehan (ed.), "The making, shaping and treating of steel", 11th Edition, Steelmaking and Refining volume. AISE Steel Foundation, Pittsburgh, USA. 1998. p. 75.
10. G.R. Belton, "How fast can we go ? The status of our knowledge of the rates of gas-liquid metal interactions". Metallurgical Transactions B, vol, 24B. April 1993. pp. 241-258.
11. E.T. Turkdogan, "Fundamentals of Steelmaking". The Institute of Materials, London. 1996.
12. R.J. Fruehan, "Nitrogen control in chromium steels". INFACON 6. Proceedings of the 1st International Chromium Steel and Alloy Congress. Cape Town, South Africa. Volume 2. SAIMM, Johannesburg, South Africa. pp. 35-41.
13. The 19th Committee on Steelmaking, The Japan Society for the Promotion of Science, "Steelmaking data sourcebook". Gordon and Breach, New York. 1988.
14. P.D. Blake, and M.F. Jordan, "Nitrogen absorption during the arc melting of iron". Journal of the Iron and Steel Institute. March 1971. pp. 197-200.
15. T. Kuwana, and H. Kokawa, "The nitrogen absorption of iron weld metal during gas tungsten arc welding". Transactions of the Japan Welding Society, vol. 17, no. 1. April 1986. pp. 20-26.
16. T. Kuwana, H. Kokawa, and K. Naitoh, "The nitrogen absorption of stainless steel weld metal during gas tungsten arc welding". Transactions of the Japan Welding Society, vol. 17, no. 2. October 1986. pp. 117-123.